J Nanostruct 16(1): 956-965, Winter 2026

RESEARCH PAPER

Synthesis and Study of ZnO, NiO and Fe_2O_3: Properties and Medical Applications

Huda Musa Mutlaq *, Ahmed K. Abbas

College of Sciences, Department of physics Wasit University, Wasit, Iraq

ARTICLE INFO

Article History:
Received 22 September 2025
Accepted 27 December 2025
Published 01 January 2026

Keywords:
AAS
Antibacterial
Fe_2O_3
NiO
Pulsed laser ablation

ABSTRACT

In this work, pulsed laser ablation with 500 and 700 mJ lasers was used to synthesis metals oxide nanoparticles from Zn, Ni, and Fe. Colloidal solutions of these metal oxides were obtained by immersing the metal in deionized water. Structural analysis, including X-ray diffraction and scanning electron microscopy, was performed. Atomic absorption spectroscopy was used to determine the initial concentration of the material. This initial concentration was then diluted into several sub-concentrations for antibacterial testing. The effects of the nanoparticles against both Gram-positive and Gram-negative bacteria were investigated.

How to cite this article
Mutlaq H., Abbas A. Synthesis and Study of ZnO, NiO and Fe_2O_3: Properties and Medical Applications. J Nanostruct, 2026; 16(1):956-965. DOI: 10.22052/JNS.2026.01.085

INTRODUCTION

Zinc oxide nanoparticles exhibit unique properties compared to conventional particles, including a hexagonal crystal structure and a wide band gap of 3.37 eV, which impart excellent electrical, optical, and catalytic properties [1]. Applications span cosmetics, sunscreens, solar cells, transparent transistors, and memory devices [2]. In addition, ZnO nanoparticles provide effective UV protection and possess environmentally friendly antibacterial activity. Furthermore, ZnO NPs are employed in the rubber industry to speed up the vulcanization process in products such as tires and gloves [3].

Nickel oxide nanoparticles are cost-effective, easy to synthesize, and simple to isolate [4]. Possessing a wide band gap (4-3.6eV), high discharge capacity (638 mAh/g), and high carrier density, these features provide superior electrochemical performance and make NiO nanoparticles highly suitable for battery Applications [5]. Due to their porous nature, NiO nanoparticles are also used as sensors for detecting compounds such as ethanol and as catalysts in reactions such as CO_2 oxidation. Additionally, Nickel oxide nanoparticles exhibit antiseptic and antibacterial properties by generating reactive oxygen species that damage microbial cell walls [6-8].

Among the iron oxides, Fe_2O_3 has attracted significant attention over the past decade due to its low cost, ease of preparation, and environmentally friendly nature. It exists in Several crystalline phases (β,α,γ,δ), with the most abundant and studied being the iron oxides(α,γ), due to their wide range applications in catalysis, gas sensing, water treatment, batteries, data storage, and biomedical fields [9][10].

Although pulsed lasers ablation is fundamentally

* *Corresponding Author Email: hudamusa@uowasit.edu.iq*

a top-down technique, the formation of nanostructures occurs through a bottom-up mechanism involving nucleation, growth, and cluster aggregation. PLA has emerged as an efficient and environmentally friendly method for synthesizing nanoparticles. When the target material is irradiated with high-power pulsed laser, it rapidly absorbs the laser energy, leading to vaporization and formation of a dense plume of ionized atoms and electrons. Consequently, a high-temperature plasma rich in ions and free electrons is formed [11-13].

E-coli is one of the most prevalent bacterial species associated human infections. It is a gram-negative bacterium that normally inhabits the gastrointestinal tract; however, certain pathogenic strains can cause severe infection, particularly the urinary and gastrointestinal system. Staphylococcus is a gram positive bacterium commonly found on the skin and mucosal surface, and is linked to a broad spectrum infections include skin and soft tissue infections, foodborne alliances and occasionally serious systemic disease. The clinical importance of these two species arises from high adaptability and decreasing resistance to multiply antibiotics, making them major target of current medical and microbiological research [14,15].

MATERIALS AND METHODS

In this part of the work, the pulsed laser ablation in liquid (PLAL) technique was used to prepare nanoparticles of zinc, nickel, and iron oxides, using deionized water as the liquid medium. First, pure pieces of zinc, nickel, and iron (1 × 1 cm^2) were placed in separate beakers, each containing 3 ml of deionized water. They were then directly exposed to a 1064 nm, 6 Hz Nd:YAG laser beam with different energies of 500 and 700 mJ, with the laser nozzle-to-target distance fixed at approximately 10 cm, as shown in Fig. 1.

The nanoparticles were characterized through a series of structural and optical investigations to accurately determine their properties. The nanoparticle solution prepared by pulsed laser ablation in liquid (PLA) was deposited onto a glass substrate placed over a hot plate using a drop-casting method, forming thin films suitable for subsequent testing. The crystalline structure of the films was analyzed using X-ray diffraction (XRD, SHIMADZU 6000) to identify the crystalline phases and evaluate the degree of crystallinity, where the crystal size is determined by the Scherrer equation.

$$D_c=\frac{K\lambda}{\beta\cos\theta} \quad (1)$$

where Dc represents the crystal size or repeating structure, β is the full width at half maximum (FWHM) in radians, Θ denotes the angle of reflection (diffraction angle) in degrees, K is the shape factor known as Scherrer's constant, usually set at 0.94, and λ denotes the wavelength of the X-rays used in the measurement. The interplanar spacing (d-spacing) is calculated using the Bragg diffraction equation, as shown below.

$$n\lambda=2d\sin\theta \quad (2)$$

Where n represents the diffraction order (often taken as 1), λ is the wavelength of the incident X-rays (e.g., 0.154 nm for Cu Kα radiation), d denotes the interplanar spacing corresponding to the Miller indices (hkl), and Θ is the Bragg angle in radians, i.e., the diffraction angle [16].

Fig. 1. PLA system.

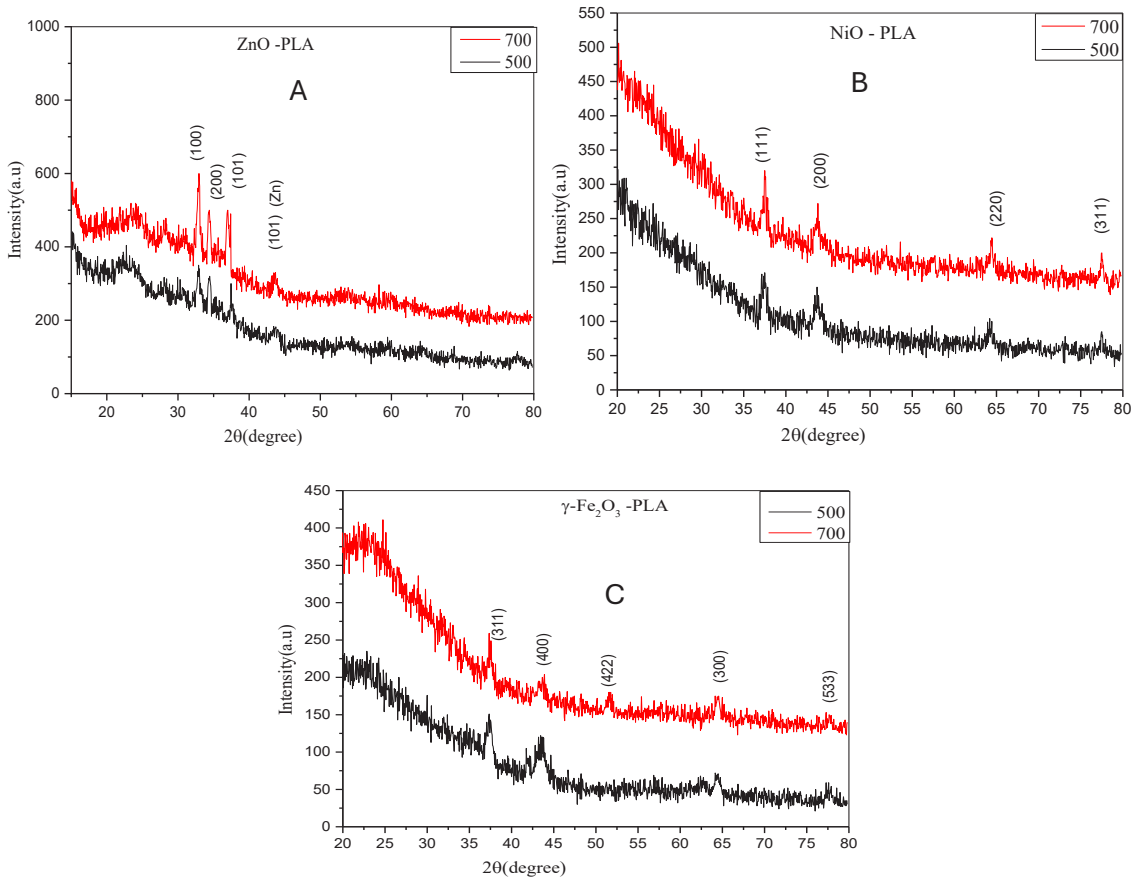

Fig. 2. X-ray diffraction for A:ZnO, B:NiO, C:γ-Fe_2O_3.

A field-emission scanning electron microscope (FE-SEM) was used to obtain accurate images of the surface topography and nanoscale morphology, providing a deeper understanding of the structural properties of the samples. The optical properties were analyzed using a Shimadzu UV-1800 UV-Vis spectrometer to determine the absorbance and optical energy gap, linking the crystal structure to the optical behavior of the prepared materials.

The initial concentrations of the prepared nanoparticles were determined using atomic absorption spectroscopy (AAS) in parts per million (ppm). These solutions were then diluted at different ratios to prepare four specific concentrations for each sample, with the aim of studying the effect of each concentration on the selected bacterial strains and evaluating their antibacterial efficacy.

Muller-Hinton (M-H) agar is prepared by adding 38 grams of the powder to 1 liter of distilled water, followed by heating on a burner with continuous stirring until fully dissolved. For 15 minutes, sterilize the M-H solution by autoclaving at 121°C. After that, the solution was allowed to reach 50°C before being poured into petri dishes and left for about 15 minutes to solidify. Once solidified, the plates are flipped upside down and kept in at 4°C.

The antibacterial activity of ZnO, NiO, and Fe_2O_3 nanoparticles prepared using pulsed laser ablation (PLA) at two different laser energies (500 and 700 mJ) was evaluated against two bacterial strains: Escherichia coli (E. coli), a Gram-negative bacterium, and Staphylococcus aureus (S. aureus), a Gram-positive bacterium, using the agar well diffusion method.

Nanoparticle solutions were prepared at different concentrations of 12.5%, 25%, 50%, and 100% for each of the two energy levels. Approximately 20 ml of sterile Muller-Hinton agar (MH) medium was poured into sterile Petri dishes.

After solidification, the active bacterial strains were inoculated using a sterile inoculation loop taken from the original cultures.

Next, 6-mm-diameter wells were created using a sterile pipette tip, and specific volumes of the prepared nanosolutions at different concentrations and energies were added to each well. The dishes were incubated at 37°C for 24 hours. After the incubation period, the average diameters of the inhibition zones were measured and recorded to assess the antibacterial efficacy of each sample based on the type of nanomaterial, laser energy, and sample concentration.

RESULTS AND DISCUSSIONS

Fig. 2 shows the X-ray diffraction patterns of zinc oxide, nickel oxide, and iron oxide prepared using pulsed laser ablation at laser energies of 500 and 700 mJ.

X-ray diffraction patterns of the three oxides prepared by PLA show the formation of pure and well-defined crystalline phases for each material. All samples exhibited a clear increase in the intensity of the diffraction peaks at higher energy levels, indicating an improvement in the degree of crystallinity and an increase in the crystal size as a result of the higher thermal energy, which provides suitable conditions for atomic arrangement within the crystal structure and reducing defects. Moreover, the crystallinity improvement increases with increasing laser energy [17].

Zinc oxide appeared in a hexagonal structure with diffraction peaks at angles 32.91°, 34.34° and 36.99°, for the (100), (002) and (101), planes, respectively. A peak belonging to zinc also appeared at angle 43.61° for the 101 planes. Both samples (500 mJ,700 mJ) are consistent with the ZnO reference according to card number (JCPDS 048-0002) and consistent with [18]. Nickel oxide exhibited a cubic crystal structure characterized by diffraction peaks positions at (37.40°,43.68°, 64.36°and 77.49°) corresponding to (111), (200), (220) and (311) the planes respectively. The diffraction patterns of both samples (500 mJ, 700

Table 1. Structural parameters of ZnO Nano oxide prepared by PLA.

Energy(mJ)	hkl	2θ (Deg.)	FWHM (Deg.)	dhkl Exp.(Å)	C.S (nm)
500	100	32.91	2.40	2.72	3.45
	002	34.44	2.70	2.60	3.08
	101	37.39	1.46	2.40	5.74
	102	43.71	2.18	2.07	3.93
700	100	32.91	1.14	2.72	7.27
	002	34.34	1.70	2.61	4.89
	101	36.99	1.64	2.43	5.11
	102	43.61	2.64	2.07	3.24

Table 2. Structural parameters of NiO Nano oxide prepared by PLA.

Energy (mJ)	hkl	2θ (Deg.)	FWHM (Deg.)	dhkl Exp.(Å)	C.S (nm)
500	111	37.38	1.04	2.40	8.06
	200	43.78	1.36	2.07	6.30
	220	64.28	0.44	1.45	21.32
	311	77.45	0.28	1.23	36.37
700	111	37.40	0.54	2.40	15.53
	200	43.68	0.89	2.07	9.62
	220	64.36	0.77	1.45	12.19
	311	77.49	0.42	1.23	24.25

Table 3. Structural parameters of Fe_2O_3 Nano oxide prepared by PLA.

Energy(mJ)	hkl	2θ (Deg.)	FWHM (Deg.)	dhkl Exp.(Å)	C.S (nm)
500	311	37.38	1.58	2.40	5.31
	400	43.49	2.08	2.08	4.11
	422	51.58	0.98	1.77	9.00
	440	64.47	0.77	1.44	12.20
	533	77.72	0.85	1.23	12.00
700	311	37.40	1.39	2.40	6.03
	400	43.53	1.95	2.08	4.39
	300	64.36	1.29	1.45	7.28
	533	77.64	0.77	1.23	13.24

Table 4. The initial concentration of samples prepared by PLAL at different laser energy.

Sample	Laser Energy (mJ)	Concentration (PPm)
ZnO	500	21
	700	40
NiO	500	15.5
	700	24.5
Fe_2O_3	500	5
	700	12

mJ) showed good agreement with the standard phase as conformed by reference card (JCPDS 47-1049) [19]. The X-ray diffraction pattern of the PLA-prepared material shows distinct diffraction peaks at angles of 35.6°, 43.53°, 64.36° and 77.64°, which are corresponding to the (311), (400), (440) and (533) crystal planes, respectively. These values are in agreement with the standard card (JCPDS card no. 39-1346) [20], confirming the formation of pure cubic phase structure. It is noted that the diffraction peak corresponding to the (442) plane appeared only in the 700 mJ sample prepared and higher laser energy which can be attributed to the improvement in crystallinity resulting from the increased laser energy, leading to greater sharpness and clarity of the diffraction peaks. With increasing laser energy during preparation, a clear improvement in the degree of crystallization and an increase in the size of the crystals was observed. The main reason for this is that the high laser energy provides a greater amount of thermal energy to the material during deposition or evaporation, which allows the atoms to move better within the crystal lattice. This additional movement reduces lattice defects and allows for the formation of larger and more regular crystals [21].

Tables 1-3 represents the XRD parameters for different oxides, the spacing between crystal planes, Miller indices, peak intensity, and maximum peak width.

Scanning electron microscopy was employed to examine the surface morphology, shape, and particle size of prepared samples. This characterization technique provides valuable insights into the influence of laser energy on the morphology and spatial distribution of nanoparticles. Moreover, it enables the evaluation of particle homogeneity of aggregation behavior and varying preparation condition. The following Figs. 3, 4 and 5 represent the SEM image of ZnO, NiO and Fe_2O_3 respectively along with the corresponding particle size distribution histograms. The mean particle size was calculated using the image software based on statistical analysis of the SEM image.

The SEM and micrographics of all synthesized oxides exhibited a similar trend with increasing laser Power. Higher laser energy promotes enhanced crystallinity and grain growth

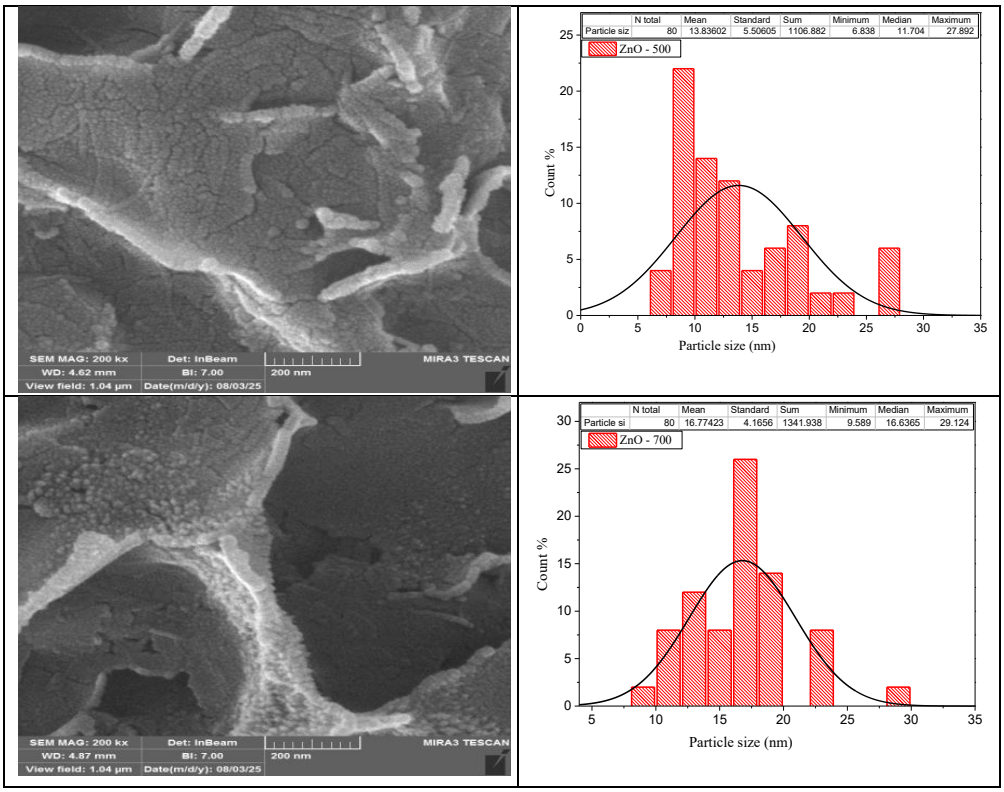

Fig. 3. SEM image for ZnO prepared by PLA.

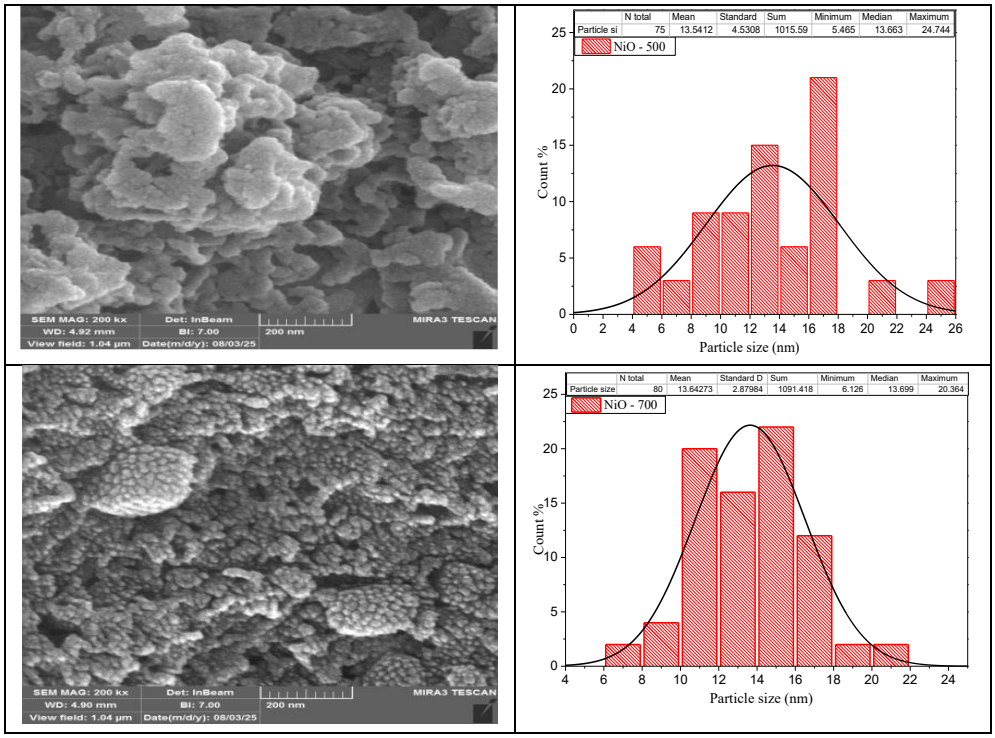

Fig. 4. SEM image for NiO prepared by PLA.

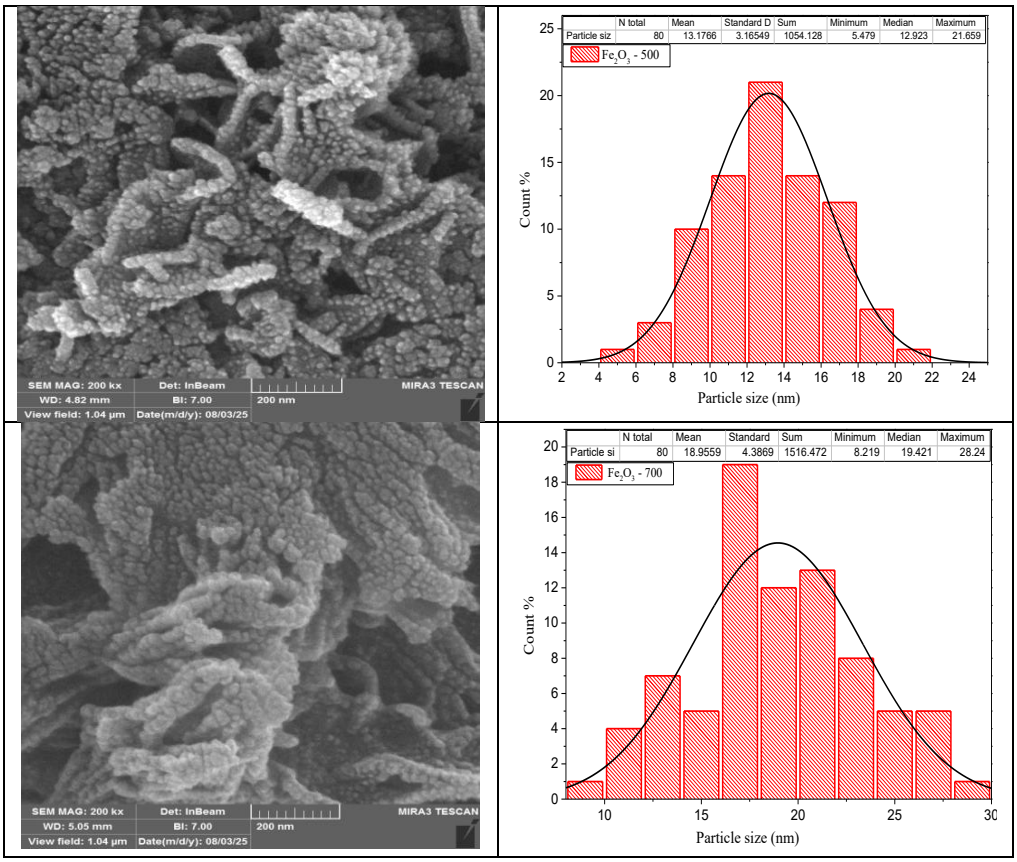

Fig. 5. SEM image for Fe_2O_3 prepared by PLA.

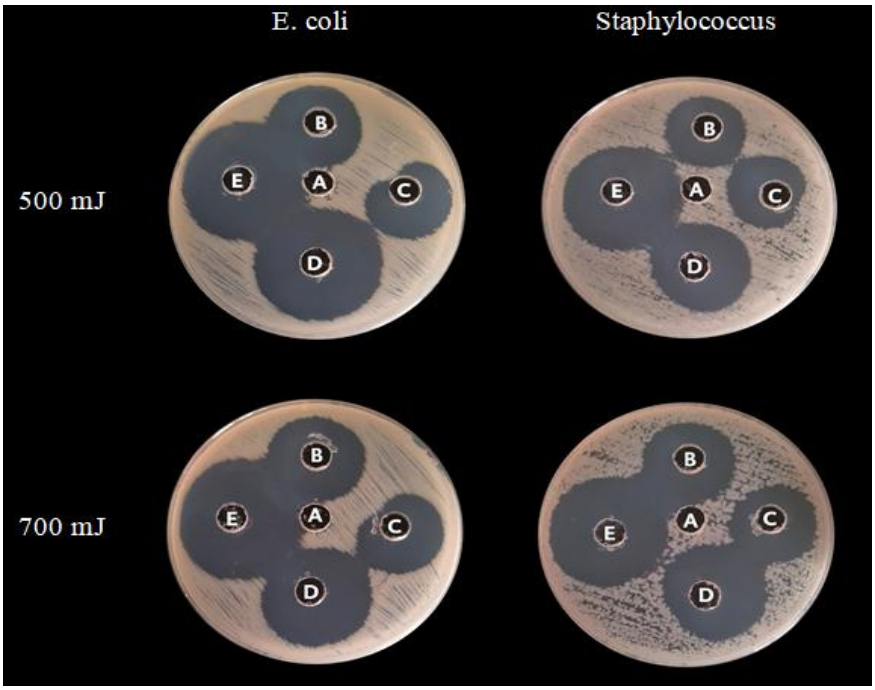

Fig. 6. Illustrate antibacterial activity against *Staphylococcus* and *E. coli* using ZnO nanoparticles prepared by PLA. A, Control. B, 12.5%. C, 25%. D, 50%. E, 100%.

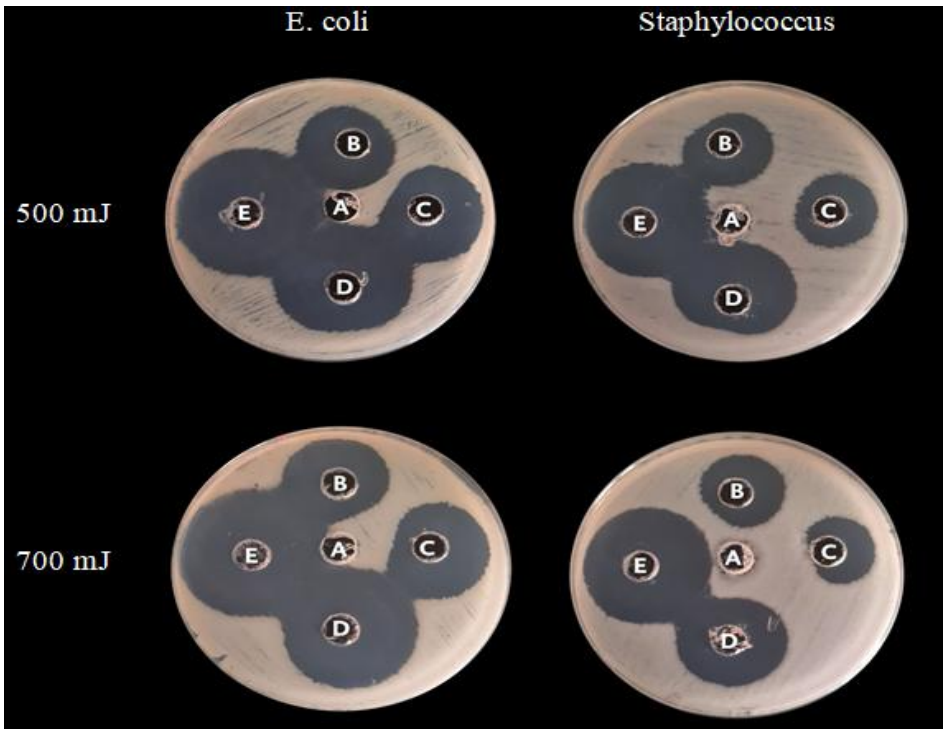

Fig. 7. Illustrate antibacterial activity against *Staphylococcus* and *E. coli* using NiO nanoparticles prepared by PLA. A, Control. B, 12.5%. C, 25%. D, 50%. E, 100%.

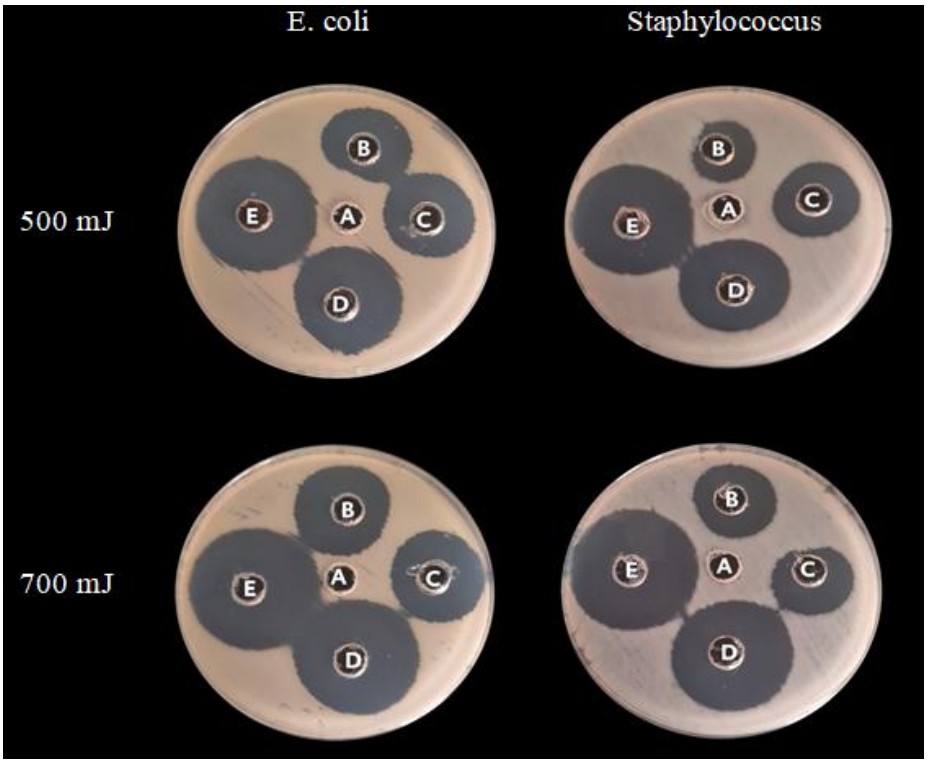

Fig. 8. Illustrate antibacterial activity against *Staphylococcus* and *E. coli* using Fe_2O_3 nanoparticles prepared by PLA. A, Control. B, 12.5%. C, 25%. D, 50%. E, 100%.

accompanied by improve particle coalescence that results in smoother and more uniform surface morphology. This behavior can be attribute to the increased thermal energy provided during ablation, which facilitates atomic diffusion and structural reorganization within the crystal lattice. Consequently, the morphological refinement indicate a significant enhancement and the physical and functional characteristic of the prepared oxide [22].

By atomic absorption spectroscopy (AAS). The Table 4 shows the concentrations of the nanoparticles synthesized in distilled water using the PLAL technique for the prepared oxides.

As the laser power in PLA technology increases, the amount of material removed from the target surface into the solution also increases. This results in the release of a greater number of atoms, thus increasing the concentration of the element in the solution. Consequently, the parts-per-million (ppm) readings increase proportionally with the laser power [23, 24].

Zinc oxide (ZnO), nickel oxide (NiO), and ferric oxide (Fe_2O_3) nanoparticles were tested at two different energies (500 mJ and 700 mJ) to evaluate their antibacterial activity. These samples were used to test their ability to inhibit the growth of both Gram-negative and Gram-positive bacteria. The results showed that the inhibition efficiency was affected by the type of nanoparticle and the laser energy used during preparation. The inhibition efficiency increased with increasing energy, which is consistent with the results of atomic absorption assays. Significant differences were also observed between the two types of bacterial cells due to differences in cell wall structure. As can be seen in the Figs. 6-8.

The figures show that with increasing oxide concentration and laser power leads to increase in the inhibition zones [25, 27]. It was also found that zinc oxide exhibits higher inhibition than other substances, attributed to its structural properties and biological activity. Furthermore, inhibition against E. coli is greater than against Staphylococcus aureus, due to the nature of the cell membrane of these bacteria [28].

CONCLUSION

This work demonstrates the success of the PLAL method in preparing nanoparticles. Increasing the laser energy led to improved crystallinity and larger crystal size, resulting in larger particle size. Furthermore, increasing the laser energy resulted in a higher concentration of suspended particles in the colloidal solution, leading to an increased inhibition zone for both Gram-negative and Gram-positive bacteria.

CONFLICT OF INTEREST

The authors declare that there is no conflict of interests regarding the publication of this manuscript.

REFERENCES

1. Islam F, Shohag S, Uddin MJ, Islam MR, Nafady MH, Akter A, et al. Exploring the Journey of Zinc Oxide Nanoparticles (ZnO-NPs) toward Biomedical Applications. Materials. 2022;15(6):2160.
2. Hazim K, Khudair ZF, Kadhim IK, Mohamed L, Hameed GF, Alyasiri FJ. Biosynthesis, Antibacterial Activity, The Photocatalytic Performance of ZnO NPS by use of Leaf Extract of the Plant Primo Fiore. Pakistan Journal of Medical and Health Sciences. 2022;16(4):456-459.
3. Dey S, Mohanty Dl, Divya N, Bakshi V, Mohanty A, Rath D, et al. A critical review on zinc oxide nanoparticles: Synthesis, properties and biomedical applications. Intelligent Pharmacy. 2025;3(1):53-70.
4. Abbas Khudhir I, Essa AF. Preparation and characterization of polypyrrole/ carbon nanotube composites using ZnO, MgO and MnO. Journal of Physics: Conference Series. 2025;2974(1):012029.
5. Abbas SA, Iqbal MI, Kim S-H, Jung K-D. Catalytic Activity of Urchin-like Ni nanoparticles Prepared by Solvothermal Method for Hydrogen Evolution Reaction in Alkaline Solution. Electrochimica Acta. 2017;227:382-390.
6. Anand GT, Nithiyavathi R, Ramesh R, John Sundaram S, Kaviyarasu K. Structural and optical properties of nickel oxide nanoparticles: Investigation of antimicrobial applications. Surfaces and Interfaces. 2020;18:100460.
7. Moya C, Ara J, Labarta A, Batlle X. Unraveling the Magnetic Properties of NiO Nanoparticles: From Synthesis to Nanostructure. Magnetism. 2024;4(3):252-280.
8. Abbas AK, Aadim KA, Jawaad MF. Spectroscopic diagnostic of (Zn:NiO) plasma by laser induced breakdown spectroscopy. AIP Conference Proceedings: AIP Publishing; 2021. p. 080013.
9. Suman, Sharma V, Devi S, Chahal S, Singh JP, Chae KH, et al. Phase transformation in Fe_2O_3 nanoparticles: Electrical properties with local electronic structure. Physica B: Condensed Matter. 2021;620:413275.
10. Aadim KA. Structural and optical properties of ZnO doped Mg thin films deposited by pulse laser deposition (PLD). Iraqi Journal of Physics. 2019;12(25):56-61.
11. Wang W, Lu L, Li Z, Xie Y. Laser induced 3D porous graphene dots: Bottom-up growth mechanism, multi-physics coupling effect and surface wettability. Appl Surf Sci. 2022;592:153242.
12. ElFaham MM, Mostafa AM, Toghan A. Facile synthesis of Cu_2O nanoparticles using pulsed laser ablation method for optoelectronic applications. Colloids Surf Physicochem Eng Aspects. 2021;630:127562.
13. Muhammed EJ, Abbas AK. Spectroscopic Assessment of

Electron Temperature and Density of Open-Air FHG Laser-Induced Zinc Titanium Plasma. International Journal of Nanoscience. 2023;23(02).
14. Hassan HJ, Abbas Ak, Ibrahim IM. Wide Range Responsivity Photodetector of Zr-Au-Ag Oxide NPs Prepared By Pulsed Laser Ablation. Journal of Physics: Conference Series. 2021;2114(1):012073.
15. Elsherif WM, Hassanien AA, Zayed GM, Kamal SM. Natural approach of using nisin and its nanoform as food bio-preservatives against methicillin resistant Staphylococcus aureus and E.coli O157:H7 in yoghurt. BMC Vet Res. 2024;20(1).
16. Kadhim FJ, Bedoui MH. Copper Oxide Nanoparticles (CuO NPs) prepared from Chitosan extract for antibacterial activity. Research Square Platform LLC; 2024. http://dx.doi.org/10.21203/rs.3.rs-4005861/v1
17. Fatimah S, Ragadhita R, Husaeni DFA, Nandiyanto ABD. How to Calculate Crystallite Size from X-Ray Diffraction (XRD) using Scherrer Method. ASEAN Journal of Science and Engineering. 2021;2(1):65-76.
18. Asaulyuk T, Saribyekova Y, Semeshko O, Kulish I. Synthesis and Structural Characterization of ZnO Nanoparticles. Herald of Khmelnytskyi National University Technical sciences. 2022;311(4):35-41.
19. Adiba, Pandey V, Munjal S, Ahmad T. NiO nanoparticles: Phase purification and strain analysis. AIP Conference Proceedings: AIP Publishing; 2021. p. 020121.
20. Dhahri R, Benamara M, Bouzidi S, Ben Moussa S, Alzahrani AYA, Nassar KI, et al. Effect of Gd doping on the microstructure and electrical characteristics of Maghemite (γ-Fe_2O_3) ceramics. J Sol-Gel Sci Technol. 2024;113(1):225-242.
21. Xu M, Liu B, Zhang L, Ren H, Gu Q, Sun X, et al. Progress on deuterated potassium dihydrogen phosphate (DKDP) crystals for high power laser system application. Light: Science and Applications. 2022;11(1).
22. Zeng Y, Li L, Huang W, Zhao Z, Yang W, Yue Z. Effect of thermal cycles on laser direct energy deposition repair performance of nickel-based superalloy: Microstructure and tensile properties. International Journal of Mechanical Sciences. 2022;221:107173.
23. Jassim AMN, Al-Kazaz FFM. Biochemical study for gold and silver nanoparticles on thyroid hormone levels in saliva of patients with chronic renal failure. European Journal of Chemistry. 2013;4(4):353-359.
24. Duque Buitrago JS, Mesa Yandy AM, Riascos Landázuri H. Investigation of laser wavelength effect on optical properties of graphene oxide colloidal nanostructures prepared by pulsed laser ablation. Journal of Physics: Conference Series. 2019;1247(1):012025.
25. Toghan A, Khairy M, Huang M, Farag AA. Electrochemical, chemical and theoretical exploration of the corrosion inhibition of carbon steel with new imidazole-carboxamide derivatives in an acidic environment. International Journal of Electrochemical Science. 2023;18(3):100072.
26. Alghamdi HM, Abutalib MM, Mannaa MA, Nur O, Abdelrazek EM, Rajeh A. Modification and development of high bioactivities and environmentally safe polymer nanocomposites doped by Ni/ZnO nanohybrid for food packaging applications. Journal of Materials Research and Technology. 2022;19:3421-3432.
27. Hadi AJ, Nayef UM, Mutlak FAH, Jabir MS. Laser-Ablated Zinc Oxide Nanoparticles and Evaluation of Their Antibacterial and Anticancer Activity Against an Ovarian Cancer Cell Line: In Vitro Study. Plasmonics. 2023;18(6):2091-2101.
28. Babayevska N, Przysiecka Ł, Iatsunskyi I, Nowaczyk G, Jarek M, Janiszewska E, et al. ZnO size and shape effect on antibacterial activity and cytotoxicity profile. Sci Rep. 2022;12(1).